Fluorescence Intensities and Lifetimes of Aromatic Hydrocarbons in Cyclohexane Solution: Evidence of Contact Charge-Transfer Interactions with Oxygen

J. Thomas Brownrigg and Jonathan E. Kenny*

Department of Chemistry, Tufts University, 62 Talbot Avenue, Medford, Massachusetts 02155

Received: August 21, 2008; Revised Manuscript Received: November 18, 2008

The fluorescence lifetimes and intensities of naphthalene, phenanthrene, chrysene, and pyrene were measured as a function of oxygen concentration in cyclohexane solution. Stern−Volmer plots of intensities and lifetimes versus oxygen concentrations revealed smaller Stern−Volmer quenching coefficients for lifetimes than for intensities. Analysis of the data in terms of static quenching models suggests that the Stern−Volmer slope differences result from a charge-transfer interaction between the aromatic and oxygen molecules in the cases of naphthalene and pyrene. A method of estimating dissolved oxygen concentration using the cyclohexane−oxygen charge-transfer band is also reported.

I. Introduction

Oxygen has long been known to quench the fluorescence of aromatic hydrocarbons. Both the fluorescence lifetime and intensity are sensitive to oxygen concentration. Oxygen is typically removed either by pumping the frozen solution while under vacuum or by purging the solution with an inert gas such as nitrogen. In his classic text, Berlman[1] published fluorescence spectra and lifetimes of many aromatic hydrocarbons in cyclohexane solution. Berlman purged his solutions with nitrogen in order to remove dissolved oxygen; however, he provided few details of the purging method. Pagano et al.[2] of this laboratory reexamined Berlman's values of F_0/F (L_0/L in Berlman's notation), the fluorescence intensity of the deaerated solution to that of an aerated solution, for chrysene, phenanthrene, naphthalene, and pyrene. The present study extends the work of Pagano et al. to include fluorescence lifetime measurements, which were not available to Pagano et al. The oxygen quenching data were analyzed using the Stern−Volmer formalism. The possible importance of contact charge-transfer complexes in explaining the static quenching component was explored.

II. Experimental Methods

All measurements described below were performed at an ambient laboratory temperature of 20 ± 1 °C. The aromatic hydrocarbons studied were naphthalene (Aldrich, 99+%), phenanthrene (Acros, 98%), chrysene (Acros, 98%), and pyrene (Acros, 98%). Pagano et al. had previously studied the same molecules, thus providing a useful comparison of relative intensities as a function of nitrogen purging time. All solutions were prepared in cyclohexane (Acros, HPLC grade, 99%) and were stored in 30 mL glass bottles with screw caps and Teflon cap liners (thickness 0.25 mm).

Solutions of the aromatic hydrocarbon were purged with nitrogen while in the fluorescence cell, a 10 mm path fused-silica cell with screw cap and septum (Starna Cells, type 3-Q-GL14-S). The top of this cell is threaded, and either a solid plastic cap or cap with rubber septum can be used. Solid caps were also purchased so that solutions could be stored for longer periods of time without solvent loss.

* To whom correspondence should be addressed. Phone: 617-627-3397. Fax: 617-627-3443. E-mail: jonathan.kenny@tufts.edu.

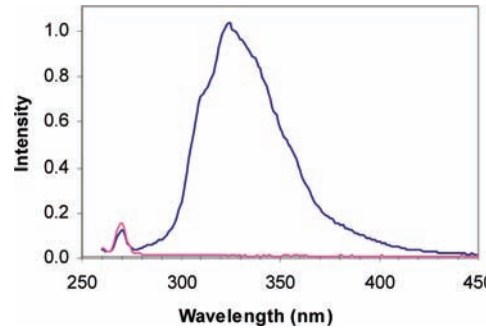

Figure 1. Fluorescence spectra of cyclohexane before (red) and after (blue) being in contact with Starna septum ~20 h. The fluorescence maximum, excited at 250 nm, is at 325 nm; the weaker band at 270 nm is the cyclohexane Raman band. The spectral bandwidths were 4 nm for excitation and emission.

Septa supplied with the cell were made of silicone rubber. It was found that when the septum was immersed in cyclohexane for approximately 1 day, fluorescent impurities from the septum leached into the cyclohexane (Figure 1). A spectrum of pure cyclohexane is shown for comparison. If the contaminant's fluorescence quantum efficiency and absorbance were the same as for naphthalene, the equivalent naphthalene concentration would be $\sim 1 \times 10^{-4}$ M.

These impurities are probably phthalates[3] added to improve septum flexibility; many phthalates are fluorescent. In order to reduce the risk of septum contamination, Teflon cap liners (thickness 0.25 mm) were inserted between the rubber septum and the cell cap. Starna septa were later replaced with septa from Restek Corp. (Thermolite septa, 12.5 mm diameter). Cyclohexane in which a Restek septum was immersed showed approximately 10-fold lower background fluorescence when excited at 250 nm than the Starna septum.

The purging procedure, similar to that of ref 2, was as follows. A 20 gauge stainless steel syringe needle with deflected tip (to avoid coring the septum) was used as the gas inlet. The needle, approximately 100 mm long, with hub removed, was connected with Teflon tubing to the gas supply. The exhaust tube was a stainless steel 25 gauge syringe needle, approximately 50 mm long with tip cut at a taper of ~20°. The exhaust needle was inserted only far enough into the cell so that the tip was visible.

10.1021/jp807495h CCC: $40.75
Published on Web 01/15/2009

The longer gas inlet needle was inserted within ~2 mm of the bottom of the cell, providing clearance for a micro stir bar (Fisher Scientific, 8 mm long × 1.5 mm diameter).

Nitrogen (ultrahigh purity, Airgas, Inc.) from a cylinder passed through a pressure regulator, needle valve, and a calibrated flow meter (Supelco flowmeter kit, 0−33 mL/min) with built-in flow control valve. The nitrogen flow rate was controlled using the meter valve and the needle valve. The cell was held vertically with clamps on a ring stand, and the center of the cell was located over a magnetic stirrer. A solution was pipetted into the cell with stir bar, and the two needles for gas inlet and outlet were inserted through the septum. Nitrogen gas was admitted to the cell, and the flow rate adjusted to approximately 5.5 ± 0.5 mL/min. For subsequent experiments (see below) in which oxygen concentrations were determined as a function of purging time, the nitrogen flow rate was 2.5 ± 0.2 mL/min. A Cary/Varian 300 dual-beam spectrophotometer was used for all absorption measurements, in particular the determination of oxygen concentrations during purging (see below). The wavelength scan rate was 600 nm/min, the spectral bandwidth was 2 nm, and the data collection interval was 1 nm.

With the use of the septum cell, the solvent loss rate was less than 0.1%/min, or about 1% loss after 10 min of purging at a nitrogen flow rate of 5.5 mL/min. This loss rate agrees well with the rate determined by Pagano et al. A 1% solvent loss, representing an apparent concentration increase, would be difficult to distinguish from fluorometer lamp power variations, typically 1−2%.

II.A. Fluorescence Measurements. An SLM 4800C spectrofluorometer was used for all fluorescence measurements. For a given purging sequence, the fluorometer gain was not changed over the course of the measurements; this avoided introducing gain nonlinearity, although the nonlinearity is relatively small. The excitation wavelength and spectral bandwidths, usually 8 nm for excitation and 1 or 2 nm for emission, were chosen to provide strong signals at different purging times without changing instrument gain. The fluorescence excitation wavelengths (nm) were for naphthalene, 265; phenanthrene, 290; chrysene, 270; pyrene, 273. These wavelengths chosen for chrysene and pyrene are shorter than used by Pagano et al. They were selected because they are located near absorbance maxima of the second absorption band, resulting in less possible interference from scattered excitation light. Two fluorescence "standards" were used during these studies. The first was tetraphenylbutadiene cast in solid poly(methyl methacrylate) (Wilmad Scientific). The fluorescence emission maximum is at 420 nm when excited at 350 nm using 4 nm spectral bandwidths. This sample was measured at the beginning and end of the day; the signal variation over a 6 h period was typically on the order of 1−2%. Fluorescence measurements conducted prior to lifetime studies used a concentrated solution of rhodamine B in ethylene glycol (8 g/L) as a reference solution. The solution was contained in a triangular cross section cell (Starna Cells, type 24-SB-Q10). The reference beam light, converted to rhodamine B fluorescence, was measured at 630 nm during the sample measurements. Subsequently, rhodamine B fluorescence was found to be temperature-dependent (7% decrease per °C increase in temperature), so a dilute solution (1000:1) of colloidal silica (Ludox SM-30) in high-purity water in a 10 cm cell served as the reference, with detection of the Rayleigh scattered excitation light. The colloidal silica solution was found to have a stability of better than 1% (−0.4% per day) when measured over a 24 h period with the SLM fluorometer. The temperature stability of the silica solution was −0.1% per °C over the range of 20−35 °C.

II.B. Lifetime Measurements. Lifetime measurements were obtained with a Photon Technologies Inc. (PTI) model TM-3 lifetime spectrofluorometer. The excitation source was a PTI model GL-3300 pulsed nitrogen laser (337.1 nm) with PTI model GL-320 dye laser and model GL-303 frequency doubler. The excitation wavelengths (nm), determined by the peak emission wavelengths of the dyes, were naphthalene, 275; phenanthrene, 290; chrysene, 268; pyrene, 272. The dye and wavelengths used for excitation were disodium fluorescein (methanol), 275; rhodamine 590 (methanol), 290; coumarin 540A (ethanol), 268 and 272. The emission wavelengths (nm) were naphthalene, 340; phenanthrene, 365; chrysene, 380; pyrene, 385. A fiber optic coupled the dye laser excitation light to the sample compartment. Light emitted by the sample was collected at right angles to the excitation beam by a fused-silica lens (focal length 37.5 mm) and focused onto the slit of a monochromator (f/4). The laser repetition rate was 10 Hz for all measurements. The emission monochromator was set near the peak of the fluorescence emission, and the monochromator bandwidth was set to the maximum value (25 nm) in order to obtain the highest signal-to-noise ratio. The instrument response function (IRF) was determined by placing a quartz diffuser plate in the sample compartment. (The IRF is the intensity distribution of the laser excitation pulse measured over the same nanosecond-scale time period used to record the fluorescence decay times.) For this data, the IRF pulse width, i.e., the full width at half-maximum intensity, was 2−3 ns.

Decay times were measured at a series of times following the excitation pulse, starting before the IRF and continuing to 200−1000 ns depending on the fluorescence lifetime. At each time "channel", the signals resulting from five laser pulses were averaged. For most decay time data, the entire time series was measured five times, and the data for each channel was averaged. For the longest purging periods (15 min total purge time), 10 time series were averaged for some of the data. For all time series, a total of 160 channels were recorded. Decay times were determined using the PTI Felix32 lifetimes application. The lifetime is calculated by reconvolution of the IRF with an exponential function, based upon an initial estimate of the lifetime. The program calculates the Marquardt χ^2 and other statistics to evaluate the goodness-of-fit to the observed decay curve. The lifetime is varied in the reconvolution process until a minimum value of χ^2 is obtained.

II.C. Dissolved Oxygen Concentrations. When cyclohexane solutions are purged with nitrogen, absorbance spectra measured with a dual-beam spectrophotometer, using an air-saturated solution as the reference, become increasingly negative below 250 nm as purging continues. If the absorption spectrum of pure cylcohexane is measured versus air (i.e., no reference sample), the absorption spectrum shows a broad, featureless band in the 190−250 nm spectral region. As the solution is purged with nitrogen, the intensity of this band decreases, until a limiting baseline absorbance is reached. The limiting baseline absorbance is due to the absorbance of the fused-silica cell, cyclohexane, and possible cyclohexane impurities; there is also a small absorbance due to light scattering at various interfaces.

Solvent absorption bands caused by the presence of dissolved oxygen have been known for over 50 years. Evans[4,5] and Munck and Scott[6] observed new absorption bands due to the presence of oxygen in both aliphatic and aromatic solvents. Tsubomura and Mulliken[7] postulated that these bands result from a "contact" charge-transfer complex formed between the organic molecule

(electron donor) and oxygen (acceptor). Munck and Scott measured the absorption spectra of oxygen in cyclohexane at three different partial pressures of oxygen in equilibrium with the liquid: 0, 0.18, and 0.84 atm. We used their data to relate the dissolved oxygen concentration to the absorbance of the charge-transfer absorption band. Munck and Scott's absorbance spectra were enlarged and digitized at intervals of 10 nm, and absorbance values for zero oxygen pressure were subtracted. Oxygen absorbance per atmosphere for the two nonzero partial pressures were calculated and averaged when possible in the spectral region of 247−210 nm, the latter being the short wavelength limit of the Munck and Scott data. Since the concentration of oxygen in cyclohexane is known (see below), the concentration of dissolved oxygen in cyclohexane could be estimated from the absorption spectrum using Munck and Scott's data.

Solubilities of oxygen (1 atm) in cyclohexane obtained from the literature are 0.0121 (30 °C);[6] 0.0114 (20 °C);[8] 0.0110 (20 °C);[9] 0.0118 (20 °C);[10] 0.0107 (20 °C);[11] 0.0113 (25 °C).[12] For conversion of oxygen solubilities in terms of mole fraction to molarities, the specific gravity of cyclohexane was taken to be 0.7786 at 20 °C, 0.7739 at 25 °C, and 0.7691 at 30 °C.[13] The average oxygen concentration obtained using these values at 20 °C is 0.0112 M. For this work, we used the oxygen solubility given in ref 8 (a critical review) at 20 °C, 0.0114 M. Assuming that air consists of 21% oxygen, the estimated concentration of dissolved oxygen in cyclohexane in equilibrium with air (1 atm) at 20 °C is 2.4×10^{-3} M. Apparent molar extinction coefficients for oxygen in air-saturated cyclohexane were calculated using the absorbance data of Munck and Scott,[6] assuming that the oxygen concentration is 2.4×10^{-3} M at 20 °C.

Absorbances of oxygen in air-saturated cyclohexane solution at 1 atm determined from Munck and Scott's data were 0.60 (210 nm); 0.28 (220 nm); 0.096 (230 nm); 0.034 (240 nm). The corresponding extinction coefficients (L mol^{-1} cm^{-1}), assuming that all oxygen molecules form charge-transfer complexes with cyclohexane molecules are 250 (210 nm); 120 (220 nm); 40 (230 nm); 14 (240 nm).

II.D. Fluorescence Intensities, Lifetimes, and Oxygen Concentrations during Purging. Values of F_0/F were initially limited to fluorescence intensity ratios measured at two oxygen concentrations in cyclohexane, the air-saturated and oxygen-free values. These studies were later expanded to include measurement of both fluorescence intensities and fluorescence lifetimes as a function of dissolved oxygen concentration while purging. The procedure was as follows. First, the absorption spectrum, fluorescence spectrum, and lifetime of the unpurged solution were obtained. After purging for a given length of time, the same three quantities were measured; after the lifetime measurement, another absorption scan was recorded. This measurement sequence was repeated after each new purging series. The following cumulative purge times (in minutes) were employed, all with nitrogen flow rate of 2.5 mL/min: 0.5, 1.5, 3, 5, 7, 9, 12, and 15. The absorption scan, covering 400−190 nm, required ∼1 min, the fluorescence scan ∼2 min, and the lifetime measurement ∼15 min. Each purging series was performed in duplicate. All data were obtained at solute concentrations 1×10^{-5} M in cyclohexane. Absorption spectra of the four aromatic hydrocarbons before and after 15 min of purging with nitrogen are shown in Figures 2−5; all spectra were recorded with a spectral bandwidth of 2 nm. The broad underlying background absorption at wavelengths <250 nm is due to the oxygen−cyclohexane contact charge-transfer band, and the absorbance of this band was used to estimate oxygen concentrations (see below). Fluorescence spectra of the same aromatic molecules before and after 15 min purging are shown in Figures 6−9; the emission spectral bandwidth was 1 nm. Fluorescence spectral intensities have been normalized to the peak intensity of the deaerated solution.

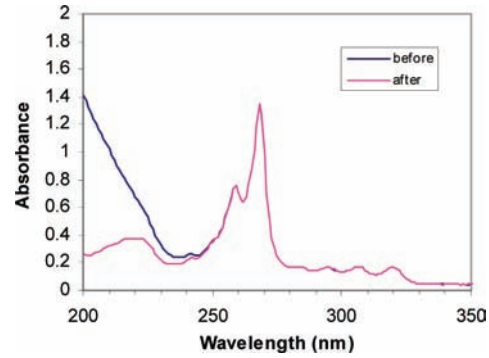

Figure 2. Chrysene, 1×10^{-5} M in cyclohexane, absorption spectra measured in a 1 cm path cell vs air reference, before and after 15 min of N_2 purge.

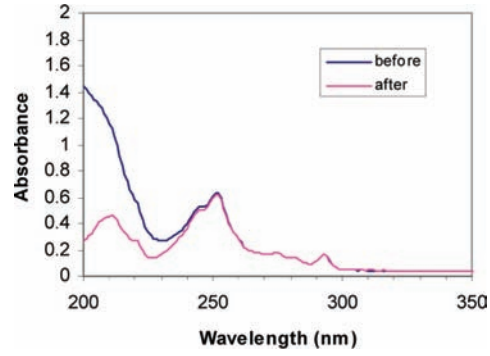

Figure 3. Phenanthrene, 1×10^{-5} M in cyclohexane, absorption spectra measured in a 1 cm path cell vs air reference, before and after 15 min of N_2 purge.

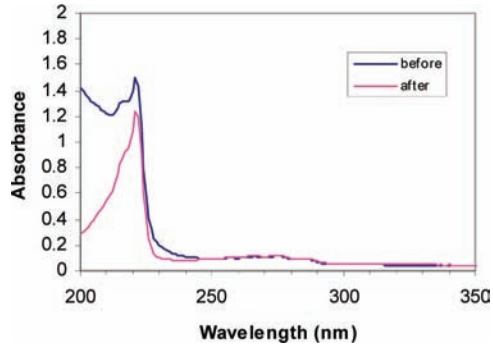

Figure 4. Naphthalene, 1×10^{-5} M in cyclohexane, absorption spectra measured in a 1 cm path cell vs air reference, before and after 15 min of N_2 purge.

Oxygen concentrations at different purging times were determined from the absorption spectra with the spectrophotometer operated in single-beam mode with no sample in the reference beam.

The baseline associated with the longest purge time, normally 15 min, was considered the "zero oxygen" spectrum, and this spectrum was subtracted from the spectra obtained at other purge times. In some cases, small shifts in baseline occurred. These shifts were probably caused either by pieces of Teflon (dislodged from the cap liner) or small gas bubbles in the light path. If the baseline shift appeared to be constant with wavelength, it was subtracted. However, the baseline was often slightly higher

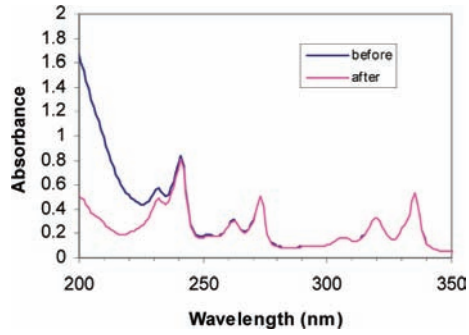

Figure 5. Pyrene, 1×10^{-5} M in cyclohexane, absorption spectra measured in a 1 cm path cell vs air reference, before and after 15 min of N_2 purge.

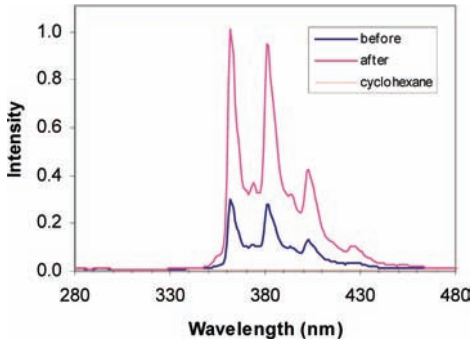

Figure 6. Chryrene, 1×10^{-5} M in cyclohexane, fluorescence spectra before and after 15 min of N_2 purge, and cyclohexane background at the same gain. Excitation wavelength 270 nm, excitation bandwidth 4 nm.

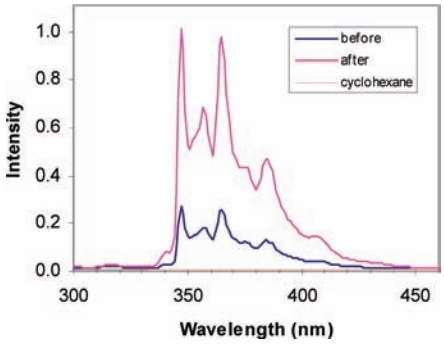

Figure 7. Phenanthrene, 1×10^{-5} M in cyclohexane, fluorescence spectra before and after 15 min of N_2 purge, and cyclohexane background at the same gain. Excitation wavelength 290 nm, excitation bandwidth 8 nm.

absorbance at shorter wavelengths and could not be subtracted. These baseline shifts sometimes resulted in an apparent negative oxygen concentration at the longest purge times, 9 and 12 min. Negative oxygen concentrations, being within one standard deviation (0.006 mM) of calculated concentrations for 9 and 12 min purge times, were assigned values of zero when calculating Stern−Volmer coefficients.

The oxygen absorbance at a given wavelength was converted to oxygen concentration using the apparent extinction coefficients from Munck and Scott as described above. Rather than use a single absorption wavelength to calculate oxygen concentration, concentrations were calculated using extinction coefficients for the wavelength range of 210−220 nm and averaged; this wavelength range was chosen because the oxygen charge-transfer band absorbance is relatively high.

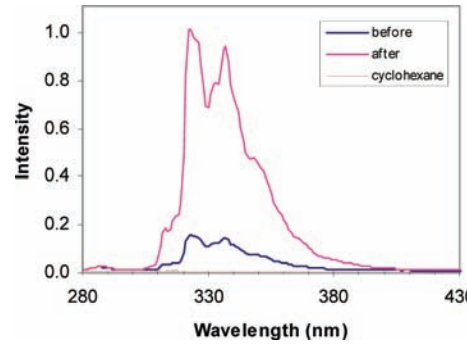

Figure 8. Naphthalene, 1×10^{-5} M in cyclohexane, fluorescence spectra before and after 15 min of N_2 purge, and cyclohexane background at the same gain. Excitation wavelength 265 nm, excitation bandwidth 8 nm.

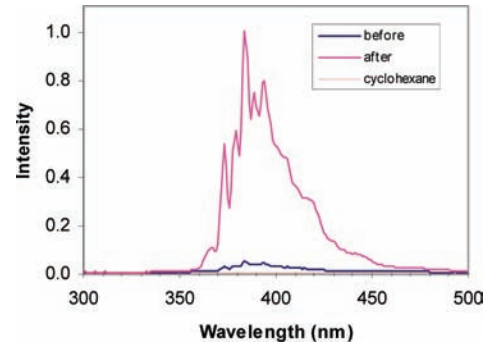

Figure 9. Pyrene, 1×10^{-5} M in cyclohexane, fluorescence spectra before and after 15 min of N_2 purge, and cyclohexane background at the same gain. Excitation wavelength 273 nm, excitation bandwidth 2 nm.

III. Results

III.A. Fluorescence Intensity Ratios. Berlman found that F_0/F is a useful predictor of the fluorescence lifetime in an oxygen-free solution, although there are some exceptions, e.g., fluoranthene. To determine F_0, the solution is normally purged with inert gas until the observed fluorescence intensity reaches an apparent maximum value. In the case of F, the corresponding intensity of an aerated solution, the actual oxygen concentration is not known explicitly; it is generally assumed that the air-saturated oxygen concentration is constant, although this might not be a good assumption due to variations in ambient atmospheric pressure. Atmospheric pressures in the Boston area in April and May 2005 when this data were taken averaged 1.001 atm, with a standard deviation 0.01 atm.[14] Thus, for our data, the assumption that the atmospheric oxygen content remained constant appears reasonable.

Values of F_0/F are given in Table 1, along with values obtained from the literature. In the present study, integrated band intensities were used to calculate F_0/F. Data in Table 1 suggest a greater precision for molecules having smaller F_0/F values, which is expected since these are less susceptible to oxygen quenching. For naphthalene and pyrene, literature values for the corresponding lifetime ratios τ_0/τ have been reported[15,16] and are included in Table 1. For pyrene, only one F_0/F value from another laboratory was found;[17] Berlman did not report a value. In general, F_0/F values obtained here are generally higher than those reported by Berlman but lower than those of Pagano et al.

The average F_0/F values in Table 1 are chrysene, 3.42; phenanthrene, 3.92; naphthalene, 6.98; pyrene 21.07. The corresponding standard deviations are chrysene, 0.20; phenanthrene 0.21, naphthalene, 0.61; pyrene, 2.1.

TABLE 1: F_0/F Values, with Standard Deviations Given in Parentheses[a]

molecule	concentration (M)	F_0/F	τ_0/τ
chrysene[b]	2.0×10^{-6} and 1.0×10^{-5}	3.45(0.03)	
chrysene[c]	8.2×10^{-5}	3.60(0.02)	
chrysene[d]	1.1×10^{-3}	3.2	
chrysene[e]	NR		3.58
phenanthrene[b]	1.0×10^{-6} and 1.0×10^{-5}	3.80(0.07)	
phenanthrene[c]	3.5×10^{-5}	4.17(0.02)	
phenanthrene[d]	1.2×10^{-3}	3.8	
naphthalene[b]	1.0×10^{-6} and 1.0×10^{-5}	6.93(0.12)	
naphthalene[c]	2.0×10^{-4}	7.62(0.07)	
naphthalene[d]	7.3×10^{-3}	6.4	
naphthalene[f]	NR		6.35
pyrene[b]	1.0×10^{-6} and 1.0×10^{-5}	22.7(0.23)	
pyrene[c]	1.7×10^{-5}	21.81(0.35)	
pyrene[g]	NR	18.7	
pyrene[e]	NR		22.5
pyrene[f]	1.0×10^{-6}–1.0×10^{-7}		18.5

[a] NR means "not reported". Values of τ_0/τ from the literature are given for comparison in the last column. [b] This work. [c] Ref 2. [d] Ref 1. [e] Ref 16. [f] Ref 15. [g] Ref 17.

III.B. Lifetimes. Lifetimes for the aromatic hydrocarbons at different oxygen concentrations are given in Table 2, which also includes values of the lifetime fitting parameter χ^2. Comparison of lifetimes obtained at the longest purge time (15 min) and values from the literature[16,18–23] are given in Table 3. Average values from two or three determinations are given. The lifetimes obtained for both the unpurged solutions and solutions purged with nitrogen for the maximum time are in good agreement with literature values.

III.C. Oxygen Concentrations. As described above, oxygen concentrations were determined by measuring the oxygen–cyclohexane charge-transfer band in the 210–220 nm region. The data of Munck and Scott were used to establish a quantitative relationship between absorbance and dissolved oxygen concentration. The concentration of oxygen in cyclohexane at 20 °C and 1 atm was taken to be 11.4 mM.

Oxygen concentrations determined for eight purging experiments (two each for each of four molecules) were averaged to determine the grand average oxygen concentration and standard deviations. The average concentrations are given in Table 4 along with the standard deviations (SD) and relative standard deviation (RSD). The oxygen concentrations were assumed to be zero for a 15 min purge time.

For all purging experiments, the nominal nitrogen flow rate was 2.5 mL/min. For the unpurged solutions, the average dissolved oxygen concentration was 2.7 mM; this is about 12% higher than the expected value 2.4 mM for an air-saturated solution. Possible sources of error include small wavelength inaccuracies and possible absorbance nonlinearities associated with different spectrophotometers. However, it is also possible that Munck and Scott's absorbance spectrum corresponding to "zero" oxygen actually contained a small amount of oxygen; if the residual oxygen concentration were 0.1 mM, the added absorbance would account for the higher observed concentrations. For the Stern–Volmer analyses below, the oxygen concentrations determined from Munck and Scott's data were scaled such that the maximum (unpurged) concentration in each purge series was 2.4 mM; scaled and unscaled oxygen concentrations are given in Table 2.

If the average unscaled oxygen concentrations in Table 4 are normalized, converted to logarithmic values, and plotted as a function of purging time, the plot is highly linear. The linear least-squares equation is $y = -0.2904x + 0.0015$, where y is $\log_{10}[O_2]$, x is the purging time in minutes, and R^2 (correlation coefficient squared) is 0.9992. From this equation, a 7 min purge reduces the oxygen concentration to 1% of its initial value, and a 10 min purge reduces the concentration to 0.1% of the initial value. However, it is important to note that the purge times given in Table 4 are *cumulative* over the duration of the experiment, and the oxygen concentrations so obtained would not necessarily be the same had the solutions been purged continuously for the same times at the same flow rate. Nevertheless, the results show that removal of dissolved oxygen is nearly exponential with purging time.

The value of the purging rate constant given in ref 2 for 5 mL/min flow rate is $k_r = 0.78$ min^{-1}; this compares with the value of 0.67 min^{-1} for the 2.5 mL/min flow rate used in this work.

III.D. Stern–Volmer Plots. Fluorescence intensities (F) and lifetimes (τ) at different purge times were plotted versus oxygen concentration. The fluorescence intensity data was expressed as the ratio F_0/F where F_0 is the intensity for an oxygen-free solution; F_0 was taken to be the intensity at the longest cumulative purge time, 15 min. Similarly, the corresponding ratio τ_0/τ is the ratio of the fluorescence lifetimes, with τ_0 corresponding to a 15 min purge time. The Stern–Volmer plot is a plot of F_0/F or τ_0/τ versus oxygen concentration.

Stern–Volmer (S–V) plots representing two purging series for each aromatic hydrocarbon are shown in Figures 10–13. For the molecules studied here, the Stern–Volmer plots for both F_0/F and τ_0/τ appeared to be nearly linear, although their slopes differ. Stern–Volmer plots were analyzed for all purging series assuming a linear relationship between the intensity or lifetime ratios and oxygen concentrations. Values of the slopes, intercepts, correlation coefficients, and standard deviations were determined using Micromath Scientist software and are summarized in Table 5. The column labeled "data SD" lists the standard deviations of the fitted data about the least-squares line. All concentrations were 1×10^{-5} M in cyclohexane, and the ambient laboratory temperature was 20–21 °C. The slope of the S–V plot for F_0/F is generally larger than that for τ_0/τ. The S–V slope ratios for intensities to lifetimes range from 1.06 for chrysene to 1.15 for naphthalene; the average value is 1.09.

The S–V slope for the lifetimes can be related directly to the dynamic quenching rate k_d, $k_d = K_d/\tau_0$, where K_d (M^{-1}) is the Stern–Volmer slope for τ_0/τ versus $[O_2]$ and τ_0 is the fluorescence lifetime in the absence of oxygen (see Lakowicz[24]). Values of k_d obtained for the four molecules range from 2.05×10^{10} to 2.15×10^{10} M^{-1} s^{-1}; the average value is 2.10×10^{10} M^{-1} s^{-1}. Saltiel and Atwater[25] used Berlman's values of F_0/F and lifetimes for their calculation of k_d for many aromatic hydrocarbons, assuming the cyclohexane air-saturated oxygen concentration to be 2.1×10^{-3} M at 20 °C. Patterson et al.[16] derived their k_d values from lifetimes, assuming an oxygen concentration 2.0×10^{-3} M at 25 °C. Values of k_d ($\times 10^{-10}$) from the literature are naphthalene, 2.67;[25] phenanthrene, 2.32;[25] chrysene, 2.32[25] and 2.9;[16] pyrene, 2.5.[16] For this work the average oxygen concentration for unpurged solutions was assumed to be 2.4×10^{-3} M, which leads to smaller values of k_d than given in the literature. If our average value of k_d (2.1×10^{10} M^{-1} s^{-1}) is adjusted to Saltiel and Atwater's oxygen concentration of 2.1×10^{-3} M, the resulting average k_d value is 2.4×10^{10} M^{-1} s^{-1}, in closer agreement with literature values. Therefore, the generally higher values of k_d from the literature are likely due to a lower assumed oxygen concentration for an air-saturated cyclohexane solution.

TABLE 2: Fluorescence Lifetimes τ (ns) Measured during Purging Series; Purge Times in Minutes, Oxygen Concentrations Millimoles per Liter[a,b]

chrysene	$[O_2]$	$[O_2]$*	τ	χ^2	chrysene	$[O_2]$	$[O_2]$*	τ	χ^2
purge time 0	2.69	2.40	14.2	1.06	purge time 0	2.67	2.40	12.6	1.23
0.5	2.10	1.88	16.2	1.12	0.5	2.06	1.85	15.2	1.18
1.5	0.96	0.85	25.8	0.98	1.5	1.06	0.95	21.8	1.00
3	0.34	0.30	37.1	0.86	3	0.34	0.30	32.4	0.97
5	0.087	0.078	43.4	1.09	5	0.094	0.085	38.5	1.01
7	0.020	0.018	45.2	0.88	7	0.027	0.024	40.7	1.05
9	0.0031	0.0028	47.1	0.84	9	0.0076	0.0068	38.1	1.02
12	0.0009	0.0008	45.5	1.22	12	0.0027	0.0025	40.3	0.88
15	0	0	48.8	1.07	15	0	0	40.8	0.85
phenanthrene	$[O_2]$	$[O_2]$*	τ	χ^2	phenanthrene	$[O_2]$	$[O_2]$*	τ	χ^2
purge time 0	2.72	2.40	14.8	1.04	purge time 0	2.69	2.40	14.3	1.32
0.5	1.95	1.72	18.1	0.8	0.5	1.96	1.75	17.6	0.93
1.5	0.92	0.81	27.6	0.89	1.5	0.92	0.82	26.6	0.92
3	0.31	0.27	39.8	0.88	3	0.31	0.27	42.7	0.94
5	0.082	0.073	47.3	0.97	5	0.063	0.056	53.3	1.08
7	0.017	0.015	51.5	0.86	7	0.013	0.011	48.3	1.69
9	0.0021	0.0019	54.7	1.03	9	−0.0016	−0.0014	53	0.9
12	−0.0017	−0.0015	ND		12	−0.0052	−0.0046	55.5	1.15
15	0	0	51.4	1.03	15	0	0	54.6	1.5
naphthalene	$[O_2]$	$[O_2]$*	τ	χ^2	naphthalene	$[O_2]$	$[O_2]$*	τ	χ^2
purge time 0	2.71	2.40	15.9	0.8	purge time 0	2.66	2.40	17.2	1
0.5	2.44	2.16	18.5	0.95	0.5	1.9	1.71	21.5	1.47
1.5	1.15	1.02	33.2	1.01	1.5	0.798	0.72	42.6	1.05
3	0.361	0.32	64.2	0.83	3	0.285	0.26	69.5	1.05
5	0.11	0.097	94.9	0.88	5	0.071	0.064	92.7	0.84
7	0.037	0.033	97.4	0.84	7	0.026	0.023	106	0.95
9	0.017	0.015	101	0.88	9	0.0087	0.0078	103	0.95
12	0.0042	0.0038	97.9	0.98	12	0.0035	0.0032	111	0.97
15	0	0	103	1.04	15	0	0	98.9	1.08
pyrene	$[O_2]$	$[O_2]$*	τ	χ^2	pyrene	$[O_2]$	$[O_2]$*	τ	χ^2
purge time 0	2.69	2.4	19.7	0.98	purge time 0	2.68	2.40	18.3	0.86
0.5	1.84	1.64	27.0	0.83	0.5	2.03	1.82	24.6	0.99
1.5	0.82	0.73	53.8	0.98	1.5	1.08	0.96	45.2	0.92
3	0.3	0.27	107	0.85	3	0.39	0.35	102	0.94
5	0.088	0.079	255	0.99	5	0.1	0.091	244	0.88
7	0.027	0.024	359	0.97	7	0.035	0.032	314	0.90
9	0.01	0.0089	385	0.85	9	0.015	0.013	368	1.02
12	0.0034	0.0031	402	0.87	12	0.0045	0.0040	398	0.91
15	0	0	391	0.87	15	0	0	386	1.10

[a] Oxygen concentrations with asterisks denote values scaled to 2.4 mM for unpurged solutions; see text. [b] ND means that no data were obtained.

TABLE 3: Fluorescence Lifetimes (ns) of Deaerated (τ_0) and Aerated (τ) Solutions, and Values from the Literature

	τ_{01}	τ_{02}	τ_{03}	τ_{0av}	τ_1	τ_2	τ_3	τ_{av}
chrysene	48.8	40.8		44.8	14.2	12.6		13.4
phenanthrene	51.4	54.6		53.0	14.8	14.3		14.6
naphthalene	103	98.9		101	15.9	17.2		16.6
pyrene	391	386	414	397	19.7	18.3	18.2	18.7
Literature Values								
naphthalene	96[a]	108[b]	120[c]		17[b]	20.4[d]		
phenanthrene	57.5[a]	56[e]						
chrysene	44.7[a]	44.7[f]			12.5[f]			
pyrene	370[b]	450[f]	400[g]	450[h]	411[i] 20[b]	20[f]		

[a] Ref 1. [b] Ref 15. [c] Ref 18. [d] Ref 19. [e] Ref 20. [f] Ref 16. [g] Ref 21. [h] Ref 22. [i] Ref 23.

TABLE 4: Average Oxygen Concentrations (mM) in Cyclohexane for Eight Purging Experiments Using the Data of Ref 6

purge time (min)	$[O_2]$ mM grand av	$[O_2]$ mM SD	$[O_2]$ mM RSD %
0	2.69	0.016	0.59
0.5	2.07	0.17	8.4
1.5	0.985	0.12	12
3	0.336	0.036	11
5	0.0886	0.015	17
7	0.0250	0.0086	34
9	0.0077	0.0065	84
12	0.00082	0.0041	500
15	0	0	

IV. Discussion

IV.A. Contact Charge-Transfer Complexes. Evans[4] noted that oxygen dissolved in aromatic solvents such as benzene and dimethylaniline revealed an additional absorption band that disappeared when the oxygen was removed. Evans' spectra showed additional absorption to longer wavelength of the solute absorption band, which Evans suggested was due to absorption by a molecular complex involving a solute molecule and oxygen. However, determination of the true maximum of the complex's absorption band was complicated by artifacts due to instrument stray light.[26] Munck and Scott[6] observed an absorption band for oxygen in cyclohexane and showed that the absorption

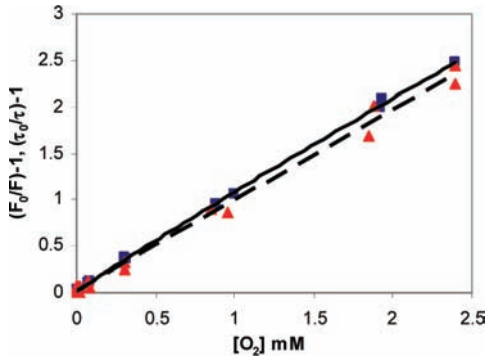

Figure 10. Stern−Volmer plots for chrysene in cyclohexane. Values of $(F_0/F) - 1$ are represented by squares and the solid line (quadratic fit), and values of $(\tau_0/\tau) - 1$ are represented by triangles and the dashed line (linear fit).

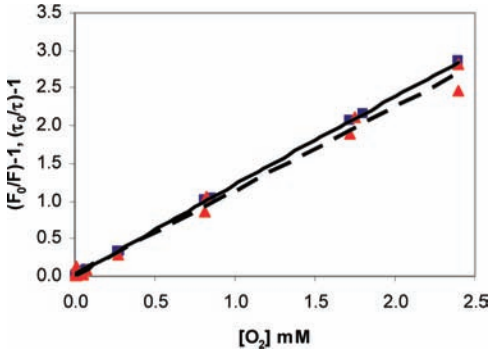

Figure 11. Stern−Volmer plots for phenanthrene in cyclohexane. Values of $(F_0/F) - 1$ are represented by squares and the solid line (quadratic fit), and values of $(\tau_0/\tau) - 1$ are represented by triangles and the dashed line (linear fit).

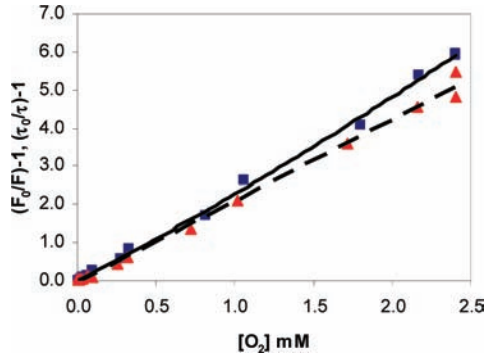

Figure 12. Stern−Volmer plots for naphthalene in cyclohexane. Values of $(F_0/F) - 1$ are represented by squares and the solid line (quadratic fit), and values of $(\tau_0/\tau) - 1$ are represented by triangles and the dashed line (linear fit).

strength of this band was proportional to the concentration of oxygen in equilibrium with the liquid. They attributed the new absorption band to formation of a 1:1 complex between oxygen and cyclohexane.

Tsubomura and Mulliken[7] measured the absorption spectra of solvents, both aromatic and nonaromatic, saturated with oxygen. Jortner and Sokolov[27] measured absorption spectra of several solvents in the presence of oxygen and nitric oxide. Absorption bands that appeared in the presence of oxygen were featureless and started at longer wavelengths than the pure solvent absorption. These spectra, like those of Evans, did not show true oxygen-induced band maxima because of limitations imposed by instrument stray light. Using molecular orbital theory, Tsubomura and Mulliken theorized that the observed

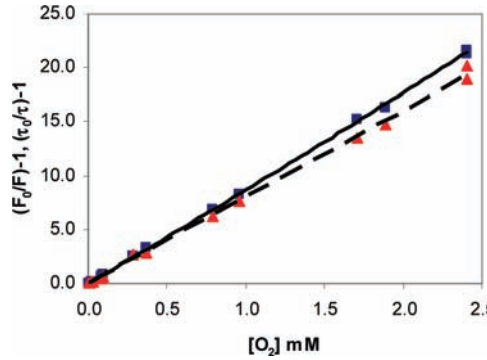

Figure 13. Stern−Volmer plots for pyrene in cyclohexane. Values of $(F_0/F) - 1$ are represented by squares and the solid line (quadratic fit), and values of $(\tau_0/\tau) - 1$ are represented by triangles and the dashed line (linear fit).

bands involve charge transfer from the organic molecule (donor) to oxygen (acceptor). They showed that there is a nearly linear relationship between the charge-transfer band energy and the donor molecule's ionization potential.

Lewis and Ware[28] studied the fluorescence oxygen quenching of pure toluene. The Stern−Volmer plots for intensities for excitation at 254 and 280 nm were nonlinear (upward curvature), whereas the Stern−Volmer plots for lifetimes were linear. The authors observed a weak absorbance in the presence of oxygen that extended to longer wavelength from the toluene absorption, similar to the oxygen contact charge-transfer bands reported by Evans and others. Lewis and Ware concluded that excitation at 280 nm results in contact charge-transfer (CCT) complex formation, which would explain the observed nonlinear Stern−Volmer plot for intensities. Their results and interpretation are consistent with ours (see below).

IV.B. Estimated Locations of Charge-Transfer Bands. There is relatively little experimental data on the electronic states and equilibrium constants involving CCT complexes with oxygen. The most extensive studies have been for benzene and naphthalene. Lim and Kowalski[29] studied the benzene−oxygen complex in the vapor phase and in carbon tetrachloride and found a broad, unstructured band with maximum at 221.5 nm. The extinction coefficient ε of this band was estimated as ~900 M^{-1} cm^{-1}; their ε value at 280 nm (~90) is in good agreement with that of Tsubomura and Mulliken. Birks et al.[30] studied the benzene vapor phase spectrum and observed the benzene−oxygen CCT band maximum at 219 nm. The authors determined the energy of formation of excited complex $^3(Bz{-}O_2)^*$ from Bz^+ and O_2^- as 2.9 ± 0.22 eV and the dipole length as 5.0 ± 0.4 Å; the ground-state complex was assumed to have a binding energy of <0.02 eV (161 cm^{-1}).

Measurements by Dijkgraaf et al.[31] and by Logunov and Rogers[32,33] on naphthalene and 1-methylnaphthalene, respectively, show the existence of a weak (ε < ~20) oxygen-induced CCT band near 350 nm. However, CCT absorption extends to shorter wavelength and overlaps the more intense bands of the free aromatic molecule, thus making it difficult to estimate the CCT band structure and maximum.

Studies of aromatic molecules in cryogenic oxygen matrixes reveal CCT bands with oxygen. Rest et al.[34] obtained spectra of benzene, toluene, styrene, and indole at 1:1 (mole ratio) mixtures with oxygen and argon at 10 K. Spectra in an oxygen matrix showed absorption bands that were not present in an argon matrix. For benzene, a single band with maximum at 235 nm was observed; the same maximum was found for oxygen/benzene ratios of 10:1 and 1:60. Following the analysis of Birks

TABLE 5: Slopes, Intercepts, and Standard Deviations for F_0/F and τ_0/τ versus [O_2] (mM) from Linear Least-Squares Fits

$(F_0/F - 1)$	slope (mM^{-1})	slope SD	intercept	intercept SD	R^2	data SD
chrysene	1.03	0.0070	0.026	0.0077	0.9993	0.025
phenanthrene	1.19	0.0060	0.0037	0.0064	0.9996	0.021
naphthalene	2.44	0.033	−0.034	0.037	0.9972	0.12
pyrene	8.90	0.043	−0.081	0.046	0.9997	0.15
$(\tau_0/\tau - 1)$	slope (mM^{-1})	slope SD	intercept	intercept SD	R^2	data SD
chrysene	0.968	0.021	0.21	0.023	0.9927	0.077
phenanthrene	1.11	0.027	0.013	0.029	0.9919	0.0.093
naphthalene	2.13	0.037	−0.038	0.041	0.9955	0.14
pyrene	8.15	0.083	−0.011	0.088	0.9985	0.29

TABLE 6: Predicted Locations (λ_{max}) from Data of Ref 35[a]

	IP (eV)	energy (eV)	λ_{max} (nm)	λ_i (nm)	λ_t (nm)
benzene	9.24	5.64	220		
naphthalene	8.14	5.17	240	265	275
phenanthrene	7.89	5.06	245	290	290
chrysene	7.6	4.93	251	270	268
pyrene	7.43	4.86	255	273	272

[a] λ_i and λ_t are the excitation wavelengths used for fluorescence intensity and lifetime measurements, respectively.

et al.,[30] Rest et al. determined that the charge separation distances (dipole lengths) in an oxygen matrix were in the range of 4.4 ± 0.3 Å for benzene; the vapor phase value is 5.0 ± 0.4 Å.

Hashimoto and Akimoto[35] obtained spectra of benzene, toluene, *p*-xylene, mesitylene, durene, styrene, and naphthalene in oxygen and argon matrixes at 11 K. The matrix mole ratio was 250:1 for benzene and the methylbenzenes and 1000:1 for styrene and naphthalene. Band maxima reported by Hashimoto and Akimoto for benzene and toluene are similar to those reported by Rest et al. The benzene−oxygen CCT band maximum in the solid oxygen matrix is shifted to the red by about 0.4 eV from the vapor phase maximum.

Charge-transfer band maxima in a solid oxygen matrix from ref 35 were used to predict the locations of the corresponding CT bands in phenanthrene, chrysene, and pyrene. Linear regression analysis gives the following relationship: $y = 0.423x + 1.28$ where x is the ionization potential and y is the CCT band energy (eV). Predicted CCT band wavelengths are given in Table 6; ionization potentials are from ref 13. In the vapor phase, CCT maxima are expected to be ~0.4 eV higher energy based on the observed red shift for benzene. Therefore, CCT maxima in solution are expected at higher energies than in a solid oxygen matrix by about 0.4 eV. For this reason, 0.4 eV was added to the calculated CCT energies; the adjusted energies and corresponding wavelengths are given in Table 6.

The two columns at the far right in Table 6 give the excitation wavelengths used to measure fluorescence intensities and lifetimes, respectively. The spectrum of naphthalene shown in Figure 2 of ref 35 indicates that the full width of the CCT band at half-maximum is ~80 nm. If the CCT bands for the other aromatics have similar widths, then the excitation wavelengths used for our data would have excited the CCT bands of these molecules.

In summary, charge-transfer band energies and intensities for aromatic hydrocarbons larger than benzene and naphthalene are difficult to estimate but are expected to depend on the location of the charge-transfer state energy in relation to strongly allowed singlet transitions. The available spectral data for contact charge-transfer complexes with oxygen suggests that the CCT band often strongly overlaps the lowest singlet transition of the free molecule. Therefore, excitation of an aromatic molecule to its lowest singlet excited state could, in many cases, result in excitation of the CCT complex as well.

IV.C. Static Quenching by Contact Charge-Transfer Complex Formation. In this section we summarize equations derived from Stern−Volmer quenching relationships; see ref 24. We assume that the fluorescence of the aromatic molecule in cyclohexane solution can be quenched either by collisions with oxygen molecules ("dynamic" quenching) or by formation of a complex, including a charge-transfer complex. Complex formation is considered a form of "static" quenching. In general, both dynamic and static quenching mechanisms may be operative, in which case the following form of the Stern−Volmer equation applies for the intensity ratio F_0/F:[24]

$$F_0/F = (1 + K[O_2])(1 + K_d[O_2]) \quad (1a)$$

$$= 1 + (K + K_d)[O_2] + KK_d[O_2]^2 \quad \text{or equivalently} \quad (1b)$$

$$(F_0/F - 1) = (K + K_d)[O_2] + KK_d[O_2]^2 \quad (1c)$$

where K_d is the dynamic quenching constant and K is the ground-state equilibrium constant for complex formation:

$$K = [MO_2]/[M][O_2] \quad (2)$$

In eq 1a, the first factor on the right $(1 + K[O_2])$ represents the reciprocal of f, the fraction of the fluorophore that remains uncomplexed. In eq 2, M denotes the aromatic molecule and MO_2 denotes a 1:1 complex with oxygen. Equation 1 assumes that the complex is nonfluorescent.

In the case of a CCT complex[36]

$$[MO_2] = a[M]_0[O_2]_0 \quad (3)$$

where the subscripts denote total concentrations and a is a constant. In this case, the fraction of fluorophore that remains uncomplexed is given by $(1 - a[O_2]_0)$; for small $a[O_2]_0$, the reciprocal of this factor is $(1+ a[O_2]_0)$. If the CCT complex concentration is small relative to the free molecule concentration and the complex is nonfluorescent

$$F_0/F = 1 + (K_d + a)[O_2] + aK_d[O_2]^2 \quad \text{or}$$

$$(F_0/F - 1) = (K_d + a)[O_2] + aK_d[O_2]^2 = A + B[O_2] + C[O_2] \quad (4)$$

where $B = (K_d + a)$ and $C = aK_d$, and A is nominally zero.

Equation 4 has the same form as eq 1, except that K is replaced by a. Under the assumptions made, a Stern−Volmer plot of F_0/F versus [O_2] cannot distinguish between a ground-state complex or a CCT complex. However, previous studies of benzene and related molecules by others suggest that association constants with oxygen are probably much less than

TABLE 7: Least-Squares Coefficients *A*, *B*, and *C* of Eq 4 for ($F_0/F - 1$) versus [O_2] (mM), Quadratic Least-Squares Fit

	A	*A* SD	*B*	*B* SD	*C*	*C* SD	R^2	data SD
chrysene	0.018	0.0071	1.10	0.026	−0.031	0.011	0.9996	0.021
phenanthrene	−0.0034	0.0054	1.25	0.019	−0.028	0.0085	0.9998	0.017
naphthalene	0.0025	0.0036	2.13	0.13	0.14	0.057	0.9980	0.11
pyrene	−0.029	0.042	8.50	0.15	0.18	0.064	0.9997	0.12

TABLE 8: Values of K_d (mM^{-1}) and *a* (mM^{-1}) Obtained from the Data, as Described in the Text

	K_d	K_d'	K_d'/K_d ratio	a_1	a_1 SD	a_2	a_2 SD	*a*
chrysene	1.13	0.968	0.86	−0.027	0.010	0.019	0.0042	−0.0044
phenanthrene	1.27	1.11	0.88	−0.022	0.0067	0.025	0.0036	0.0016
naphthalene	2.07	2.13	1.03	0.066	0.028	0.035	0.0082	0.050
pyrene	8.47	8.15	0.96	0.022	0.0076	0.041	0.0056	0.031

one. Therefore, it seems reasonable to consider static quenching as being a consequence of contact charge transfer.

From ref 24, the following relationship involving lifetime and intensity ratios may be derived:

$$(F_0/F)/(\tau_0/\tau) \sim (1 - a[O_2])^{-1} \sim 1 + a[O_2] \quad (5)$$

For eq 5 to be valid the oxygen concentrations must be the same for both intensity and lifetime measurements. Because these measurements were taken sequentially, there were small differences in oxygen concentrations. As a means of correction, the Stern−Volmer equations for (τ_0/τ) versus [O_2], based on a linear least-squares fit, were used to estimate the values of (τ_0/τ) for oxygen concentrations corresponding to the (F_0/F) values.

IV.D. Static Quenching Constants from the Data. Equations 4 and 5 were applied to the intensity ratios F_0/F and intensity/lifetime ratios $(F_0/F)/(\tau_0/\tau)$ in order to determine the constant *a*. Plots of ($F_0/F - 1$) versus [O_2] were analyzed by quadratic least-squares fits using Micromath Scientist. Values of the quadratic coefficients, standard deviations, and R^2 values are listed in Table 7. Results obtained based on linear least-squares fits versus [O_2] are given in Table 5. Data from two purging experiments were combined for a total of 17 measurements. As for the data in Table 5, oxygen concentrations for each purging series were scaled such that the oxygen concentration of the unpurged solution was 2.4 mM.

Values of K_d and *a* were derived from the quadratic least-squares coefficients *A* and *B* by solving two simultaneous equations involving the linear and quadratic terms of eq 4. The values of *a* obtained from quadratic least-squares coefficients are designated a_1 in Table 8.

The constant *a* was also determined from the slope of $(F_0/F)/(\tau_0/\tau)$ versus [O_2] as given in eq 5, assuming *a* is much less than unity. In actuality, values of $(\tau_0/\tau)/(F_0/F)$ were plotted against [O_2] since this relationship should be directly linear in [O_2]. The values of *a* thus obtained, designated a_2, are given in Table 8. The average of the values a_1 and a_2 obtained from the two different analyses is designated *a*. Values of K_d obtained from quadratic least-squares fits of ($F_0/F - 1$) versus [O_2] are given in the first column; values obtained from linear least-squares fits of ($\tau_0/\tau - 1$) versus [O_2], designated K_d', are given in the second column, and the ratio of the two values is given in the third column.

The values of the interaction constant *a* obtained are subject to considerable error, as evidenced by large relative standard deviations. However, the values of *a* for naphthalene and pyrene appear to be larger and more significant than the corresponding values for phenanthrene and chrysene. If correct, this implies that a small quadratic term is present in the plot of F_0/F versus [O_2] for naphthalene and pyrene. Existence of a quadratic term suggests that, in addition to a large dynamic quenching component, a much smaller static component is also present.

A reasonable explanation of the static quenching component is that the aromatic molecules form contact charge-transfer complexes with oxygen. As discussed previously, there is a large body of experimental evidence that supports the existence of CCT transitions in both aromatic and nonaromatic molecules. The value of the CCT quenching constant *a* is in the range of approximately 0−50 M^{-1} (0−0.05 mM^{-1}) for the molecules studied. The dynamic quenching coefficients, on the other hand, are in the range of ∼1000−8000 M^{-1}.

Ware,[37] in a study of oxygen quenching of anthracene, 9,10-dichloroanthracene, 9,10-diphenylanthracene, and perylene, found that the quenching constants derived from Stern−Volmer intensity relationships averaged approximately 7% greater than those derived from lifetimes. Ware attributed the difference to the use of a phase-shift method to determine lifetimes, which underestimated the values of the diffusion constants. We obtain an average slope ratio of 9% greater for the four molecules, in approximate agreement with Ware's value, although our lifetimes were measured by a time-gated pulse method.

Lakowicz and Weber[38] studied the oxygen quenching of fluorescence in aqueous solution at pressures up to 100 atm. Included in their study were 2-methylanthracene, 9-vinylanthracene, and perylene in dodecane solution. For these molecules the ratios of the static to dynamic quenching constant were in the range of 2.6−4.6%, which is similar to 2% obtained here for naphthalene (and even less for the other aromatics). In contrast, the corresponding ratios for polar fluorophores in *aqueous* solution were much smaller (and in some cases negative), leading the authors to conclude that there was no significant static quenching by oxygen in aqueous solution. The authors noted that perylene in dodecane solution showed no change in absorption spectrum at oxygen pressures of 100 atm. However, the nonlinear behavior of the perylene Stern−Volmer intensity plot (upward curvature) implied the existence of a complex, or "sphere-of-action" quenching. For perylene in dodecane their data indicated a sphere-of-action distance equal to 9 Å. Regarding the apparent lack of change in the perylene spectrum with oxygen pressure, their spectrum of pure dodecane shows that solvent absorption becomes very strong below ∼270 nm and could mask changes in perylene absorption at shorter wavelengths.

Canuel et al.[39] studied the fluorescence quenching of aromatic molecules by both oxygen and halogenated organics in toluene solution. The aromatics studied were anthracene, perylene, ovalene, dibenzo[*a*, l]pentacene, and Exalite 404 (a laser dye). For oxygen quenching, the Stern−Volmer plots for both intensities and lifetimes appeared linear up to oxygen concentrations of 7.4×10^{-3} M at 20 °C for oxygen pressure 1 atm. Stern−Volmer intensity slopes were greater than those for lifetimes for anthracene, perylene, and Exalite 404; the slope ratios were, respectively, 1.02, 1.21, and 1.18. These slope ratios are somewhat larger than obtained in our work (average 1.09, standard deviation 0.04). For the case of quenching by halogenated compounds, the lifetime slope sometimes exceeded the intensity slope so that Canuel et al. concluded that the slope differences were due to experimental uncertainties. The authors considered a sphere-of-action quenching model (see below), but concluded that for all molecules except Exalite 404 (shortest lifetime) this model predicted "unrealistically large and varying radii of interactions". These authors concluded that quenching

by oxygen is mainly dynamic (diffusion-controlled), whereas quenching by halogenated molecules apparently involves mixing of the lowest excited states of aromatic and quencher.

IV.E. Discussion of Binding in Oxygen Complexes. For the aromatic molecules studied in this work, binding energies to O_2 in the ground state have not been investigated, either theoretically or experimentally. Again, the only system for which appreciable data are available is benzene−O_2. For this complex, Grover et al.[40] measured a ground-state dissociation energy D_0 of 6.90 kJ/mol by photoionization in a molecular beam, corresponding to a room-temperature enthalpy of formation of about −4.0 kJ/mol. Using entirely different methodology (temperature dependence of equilibrium constants in static gas), Casero and Joens[41] determined an enthalpy of formation at 298 K of −4.3 kJ/mol for the same complex. Ab initio calculations by Granucci and Persico[42] gave a D_0 of 4.4 kJ/mol, but the authors suggest correcting it upward to 5.4 kJ. Collectively, these three references are in approximate agreement that the room-temperature stabilization energy of the complex relative to benzene + O_2 is less than $2RT$. Older estimates[30,43] suggest an even weaker bond. All these reports are consistent in characterizing the benzene−oxygen interaction as a "loose" or "contact charge-transfer" complex. Complexes of O_2 with larger aromatics have been observed in spectroscopic experiments conducted in helium nanodroplets. Lehmann and co-workers report observations of O_2 complexes with perylene,[44] benzo[*g*,*h*,*i*]-perylene,[45] and coronene,[45] but no binding energy data are available. Curiously, Graf et al.[46] report the failure to observe O_2 complexes with anthracene and 9,10-dicyanoanthracene in supersonic jet expansions, despite observing complexes of these aromatics with Ne, Ar, and CO_2. They estimate that a binding energy around 16 kJ/mol (corresponding to that calculated for anthracene−Ar) might be required to observe the complex under their experimental conditions. Qualitatively, one might expect the O_2 complex to be roughly as tightly bound as the Ar complex, because their static polarizabilities are nearly equal. However, given the failure to observe the complexes, it may be that the binding energy of O_2 with any of these planar aromatics is approximately equal to that of O_2−benzene, since the O_2 (which lies above the ring with its axis parallel to the plane of carbon atoms in the benzene complex) cannot interact significantly with more than one six-membered ring. Thus, the available "chemical" evidence seems to support the picture of a very loosely bound contact charge-transfer complex. Parsons and Chandler[47] have studied van der Waals complexes of cyclohexane with O_2 and Cl_2. Excitation of these complexes into the contact charge-transfer bands leads to the production of atomic oxygen and chlorine fragments. Although beyond the scope of our work, their results and references cited therein demonstrate the importance of contact charge-transfer states in energy transfer processes.

IV.F. Sphere-of-Action Quenching. Lakowicz[24] considers two static quenching mechanisms, complex formation and sphere-of-action quenching. Complex formation implies that oxygen forms a weak complex with the aromatic molecule and that this complex is essentially nonfluorescent. The sphere-of-action model assumes that an oxygen molecule, when within a certain distance of the aromatic, quenches fluorescence by an unspecified mechanism.

Lakowicz[24] gives the following expression for sphere-of-action quenching:

$$F_0/F = (1 + K_d[Q])\exp([Q]\upsilon N/1000) \quad (6)$$

where K_d is the diffusion constant, υ is the volume of the interaction sphere in cm^3, [Q] is the quencher concentration (M), and N is Avogadro's number; N/1000 is a conversion factor from units of mol/liter to molecules/cm^3. Since the first factor in this expression is the Stern−Volmer lifetime ratio, eq 6 can be rewritten

$$(F_0/F)/(\tau_0/\tau) = \exp([Q]\upsilon N/1000) \quad (7)$$

The sphere-of-action model predicts an exponential dependence with quencher concentration. Quenching involving complex formation should, to a first approximation, result in a Stern−Volmer F_0/F plot that is quadratic in oxygen concentration.

If the exponential term is small compared to unity, eq 6 can be written

$$(F_0/F)/(\tau_0/\tau) \sim 1 + ([Q]\upsilon N/1000) = 1 + V[Q] \quad (8)$$

The term V can be considered as a volume per molecule so that, if this volume is a sphere, the corresponding radius (angstroms) is given by

$$R = 10(V/2.52)^{1/3} \quad (9)$$

The form of eq 8 is similar to eq 5, which relates $(F_0/F)/(\tau_0/\tau)$ to oxygen concentration for small values of the CCT constant a. Therefore, the values of a derived above can be used to obtain values of the sphere-of-action radius R. Taking V to be the values of a_1 and a_2 given in Table 8, values of R range from 20 Å for chrysene to 27 Å for naphthalene. These interaction distances are 3−4× greater than the 6 Å intermolecular separation assumed for dynamic quenching by oxygen (ref 37) and are also much greater than the 5 Å separation calculated for the benzene−oxygen charge-transfer complex (ref 30). Therefore, the sphere-of-action model predicts interaction distances that are much larger than expected.

V. Conclusions

The existence of a CCT complex between oxygen and the aromatic molecule could explain the difference in Stern−Volmer slopes for F_0/F and τ_0/τ versus [O_2]. We derived Stern−Volmer equations for the case of dynamic and static quenching assuming the fluorophore forms an oxygen CCT complex and derived values of the CCT coefficient a. The values of a obtained from the data are in the range of ∼0 to 50 M^{-1}. Since the maximum oxygen concentration in cyclohexane solution was 2.4×10^{-3} M, and the concentrations of the aromatic molecules were 1×10^{-5} M, the estimated maximum concentration of the CCT complex is $\sim 1.2 \times 10^{-6}$ M, assuming a value of 50 M^{-1} for the CCT coefficient a; thus, at most about 12% of the aromatic molecules form CCT complexes.

Unfortunately, there is little data from the literature allowing an estimate of CCT band extinction coefficients. The maximum extinction coefficient determined for liquid benzene is ∼900 M^{-1} cm^{-1} at 222 nm;[29] the corresponding value in a solid oxygen matrix is 5400 M^{-1} cm^{-1}.[35] For benzene, alkyl benzenes, and naphthalene the CCT band in an oxygen matrix overlaps the lowest singlet absorption band of the free molecule, making it difficult to observe the CCT band. If the CCT band is assumed to have an extinction coefficient of 5000 M^{-1} cm^{-1} at the wavelength used to excite fluorescence, and the CCT constant a is 50 M^{-1}, the calculated CCT band absorbance for a 1 cm path cell is 0.006 for a solute concentration of 1×10^{-5} M in an air-saturated cyclohexane solution. This absorbance is not much greater than the root-mean-square noise level (∼0.001) of the spectrophotometer used in our study. Since CCT extinction coefficients observed in a solid oxygen matrix are likely to be larger than those in solution because of smaller

intermolecular distances, extinction coefficients in solution are likely to be even smaller.

Excitation wavelengths used for data in this study probably excited both the free molecule and the CCT complex, although the extent of CCT excitation is unknown. It would be informative to conduct similar studies on molecules whose CCT band shapes were known relative to the free molecule bands. Excitation with different wavelengths should result in different Stern−Volmer intensity slopes depending upon the relative absorption of free and complexed molecules. For these studies, use of higher oxygen concentrations would be desirable since differences in the lifetime and intensity Stern−Volmer slopes should be greater, permitting more accurate measurements of the contact charge-transfer constants.

Acknowledgment. The authors thank Todd Pagano for helpful suggestions relating to earlier studies of nitrogen purging methods performed with Adam Biacchi. We also thank Kerin Clow for assistance with fluorescence decay time measurements and with analysis of fluorescence lifetimes.

References and Notes

(1) Berlman, I. B. *Handbook of Fluorescence Spectra of Aromatic Molecules*, 2nd ed.; Academic Press: New York, 1971.
(2) Pagano, T.; Biacchi, A. J.; Kenny, J. E. *Appl. Spectrosc.* **2008**, *62*, 333–336.
(3) Restek Corporation, 110 Benner Circle, Bellefonte, PA 16823, 2004 catalog, p 108.
(4) Evans, D. F. *J. Chem. Soc.* **1953**, 345–347.
(5) Evans, D. F. *J. Chem. Soc.* **1957**, 1351–1357.
(6) Munck, A. U.; Scott, J. F. *Nature* **1956**, *177*, 587.
(7) Tsubomura, H.; Mulliken, R. S. *J. Am. Chem. Soc.* **1960**, *82*, 5966–5974.
(8) Battino, R.; Rettich, T. R.; Tominaga, T. *J. Phys. Chem. Ref. Data* **1983**, *12*, 163–178.
(9) Novak, K. *Chem. Abstr.* **1963**, *58*, 69833.
(10) Luhring, P.; Schumpe, A. *J. Chem. Eng. Data* **1989**, *34*, 250–257.
(11) Wild, J. D.; Sridhar, T.; Potter, O. E. *Chem. Eng. J. (Amsterdam)* **1978**, *15*, 209–214.
(12) Guerry, D. *Ind. Eng. Chem. Data* **1958**. *3*, 166 cited in ref 11.
(13) NIST Chemistry WebBook, NIST Standard Reference Database No. 69, June 2005 release. http://webbook.nist.gov/chemistry.
(14) National Data Buoy Center Station 44013, 16 nautical miles east of Boston, MA. http://www.ndbc.noaa.gov/station_history.php?station=44013.
(15) Hautala, R. R.; Schore, N. E.; Turro, N. J. *J. Am. Chem. Soc.* **1973**, *95*, 5508–5514.
(16) Patterson, L. K.; Porter, G.; Topp, M. R. *Chem. Phys. Lett.* **1970**, *7*, 612–614.
(17) Rollie, M. A.; Patonay, G.; Warner, I. M. *Ind. Eng. Chem. Res.* **1987**, *26*, 1–6.
(18) Mataga, N.; Tomura, M.; Nishimura, H. *Mol. Phys.* **1965**, *9*, 367–375.
(19) Birks, J. B.; Leite, M. S. S. C. P. *J. Phys. B: At. Mol. Phys.* **1970**, *3*, 417–424.
(20) Amata, C. D.; Burton, M.; Helman, W. P.; Ludwig, P. K.; Rodemeyer, S. A. *J. Chem. Phys.* **1968**, *48*, 2374–2376.
(21) Kikuchi, K. *Chem. Phys. Lett.* **1991**, *183*, 103–106.
(22) Birks, J. B.; Dyson, D. J.; Munro, I. H. *Proc. R. Soc. London, Ser. A* **1963**, *275*, 575–588.
(23) James, D. R.; Siemiarczuk, A.; Ware, W. R. *Rev. Sci. Instrum.* **1992**, *63*, 1710–1716.
(24) Lakowicz, J. R. *Principles of Fluorescence Spectroscopy*, 3rd ed.; Springer Science+Business Media: New York, 2006; pp 280−286.
(25) Saltiel, J.; Atwater, B. W. Spin-Statistical Factors in Diffusion-Controlled Reactions. In *Advances in Photochemistry*; Volman, D. H., Hammond, G. S., Gollnick, K., Eds.; Wiley-Interscience: New York, 1988; Vol. 14, pp 1−90.
(26) Evans, D. F. *Chem. Ind.* **1953**, *13*, 1061.
(27) Jortner, J.; Sokolov, S. *J. Phys. Chem.* **1961**, *65*, 1633–1635.
(28) Lewis, C.; Ware, W. R. *J. Chem. Soc., Faraday Trans. 2* **1976**, *72*, 1851–1859.
(29) Lim, E. C.; Kowalski, V. L. *J. Chem. Phys.* **1962**, *36*, 1729–1732.
(30) Birks, J. B.; Pantos, E.; Hamilton, D. S. *Chem. Phys. Lett.* **1973**, *20*, 544–546.
(31) Dijkgraaf, C.; Sitters, R.; Hoijtink, G. J. *Mol. Phys.* **1962**, *5*, 643–644.
(32) Logunov, S. L.; Rodgers, M. A. J. *J. Phys. Chem.* **1992**, *96*, 2915–2917.
(33) Logunov, S. L.; Rodgers, M. A. J. *J. Phys. Chem.* **1993**, *97*, 5643–5648.
(34) Rest, A. J.; Salisbury, K.; Sodeau, J. R. *J. Chem. Soc., Faraday Trans. 2* **1977**, *73*, 265–273.
(35) Hashimoto, S.; Akimoto, H. *J. Phys. Chem.* **1989**, *93*, 571–577.
(36) Orgel, L. E.; Mulliken, R. S. *J. Am. Chem. Soc.* **1957**, *79*, 4839–4846.
(37) Ware, W. R. *J. Phys. Chem.* **1962**, *66*, 455–458.
(38) Lakowicz, J. R.; Weber, G. *Biochemistry* **1973**, *12*, 4161–4170.
(39) Canuel, C.; Badre, S.; Groenzin, H.; Berheide, M.; Mullins, O. C. *Appl. Spectrosc.* **2003**, *57*, 538–544.
(40) Grover, J. R.; Hagenow, G.; Walters, E. A. *J. Chem. Phys.* **1992**, *97*, 628–642.
(41) Casero, J. J.; Joens, J. A. *J. Phys. Chem. A* **1997**, *101*, 2607–2609.
(42) Granucci, G.; Persico, M. *Chem. Phys. Lett.* **1993**, *205*, 331–336.
(43) Gooding, E. A.; Serak, K. R.; Ogilby, P. R. *J. Phys. Chem.* **1991**, *95*, 7868–7871.
(44) Çarçabal, P.; Schmied, R.; Lehmann, K. K.; Scoles, G. *J. Chem. Phys.* **2004**, *120*, 6792–6793.
(45) Birer, O.; Moreschini, P.; Lehmann, K. K. *Phys. Chem. Chem. Phys.* **2008**, *10*, 1648–1657.
(46) Graf, U.; Niikura, H.; Hirayama, S. *J. Phys. Chem. A* **1997**, *101*, 1292–1298.
(47) Parsons, B. F.; Chandler, D. W. *J. Phys. Chem. A* **2003**, *107*, 10544–10553.

JP807495H